Narrow Linewidth Hybrid Square/Rhombus-rectangular Microcavity Lasers

Meng-Wei Sheng , You-Zeng Hao, Wei Wang, Yue-De Yang, Jin-Long Xiao, and Yong-Zhen Huang
Institute of Semiconductors,
Chinese Academy of Sciences,
Beijing, China
Center of Materials Science and Optoelectronics Engineering,
University of Chinese Academy of Sciences
Beijing, China
yzhuang@semi.ac.cn

***Abstract*—We demonstrate a kind of narrow linewidth hybrid square/rhombus-rectangular microcavity lasers prepared with 3-quantum wells AlGaInAs/InP epitaxial wafers. The device fabricated by standard projection i-line lithography fabrication process shows a maximum single-mode fiber output power of 10 mW and a narrow linewidth of 500 kHz.**

Keywords—semiconductor laser, hybrid square/rhombus-rectangular microcavity, narrow linewidth.

I. Introduction

Narrow linewidth lasers are essential for a wide range of applications such as coherent optical communication [1, 2], light detection and ranging (LIDAR) [3], and atomic clocks [4]. To meet the increasing demand for network capacity, advanced modulation formats with stringent phase stability requirements have emerged in coherent optical communications, meaning that the laser linewidths are required to be narrower. For instance, 16-state quadrature amplitude modulation (16QAM) can require linewidths in the order of 100 kHz [5, 6]. Light sources for coherent optical communication are tending towards easy integration, chip scale, low cost, and low power consumption, making monolithic semiconductor lasers potentially promising.

Mode coupling between a square microcavity and a Fabry-Perot (FP) cavity has been investigated [7]. In this work, we report a hybrid square/rhombus-rectangular laser at 1550 nm. The laser is fabricated by standard projection i-line lithography fabrication process. Single-mode operation with narrow linewidth is achieved by reducing the longitudinal confinement factor.

II. Device Structure and Fabrication

The schematic structure of the HSRRL is shown in Fig. 1(a) as in [8], which consists of a square/rhombus microcavity (SRM) and an FP cavity. The SRM shown in Fig. 1(b) as a deformed square microcavity with a vertex extending a

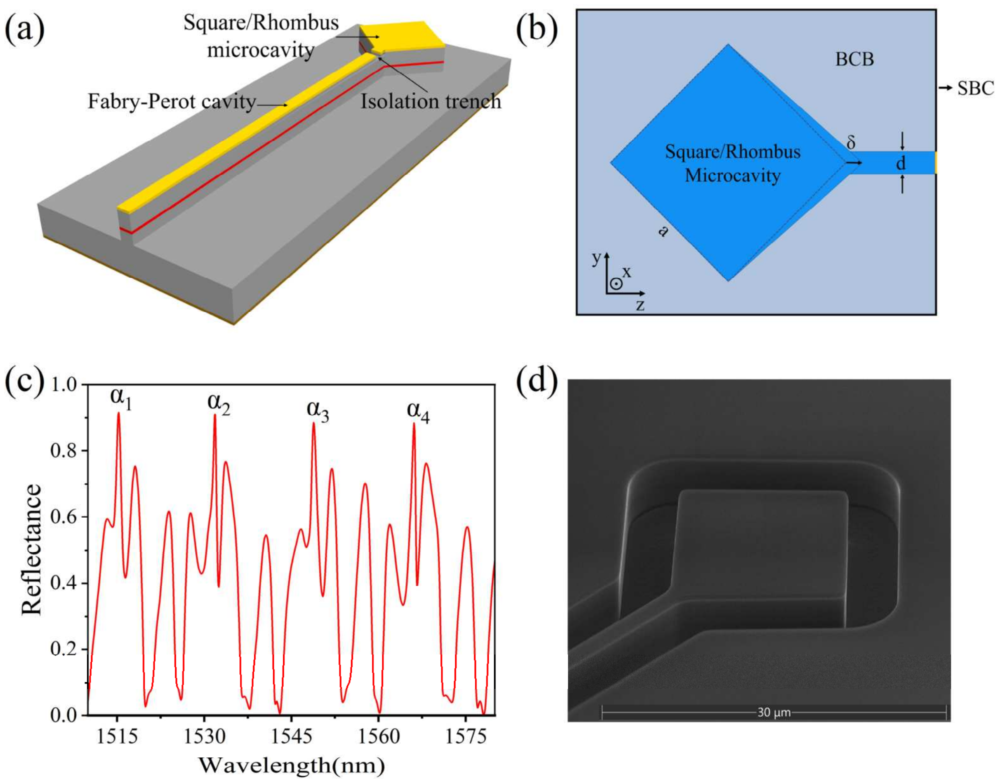

Fig. 1. (a) The schematic structure of HSRRL. (b) Schematic diagram of a 2D SRM. (c) The simulated reflectance spectrum of the SRM with a = 15 μm, δ = 0.82 μm, and d = 2 μm. (d) The scanning electron microscopic images of an HSRRL after ICP etching.

distance of δ acts as a selective equivalent reflective end facet of the FP cavity. The reflectance of the proposed SRM is simulated by the two-dimensional finite element method (FEM) [9]. The refractive index of the microcavity is set to 3.2 and the laterally surrounded medium is bisbenzo cyclobutene (BCB) with a refractive index of 1.54. The scattering boundary condition (SBC) is placed on the periphery of the BCB to absorb the plane wave scattered by the cavity. The numeric port was added at the input of the waveguide, such that the lightwave is excited at the port. Here, the transverse-electric (TE) mode is considered, as the TE polarization dominates the modal gain in the experimental compressively strained multi-quantum wells (MQWs) wafers. The side length of the SRM, the vertex extending distance, and the width of the waveguide are taken to be a = 15 μm, δ = 0.82 μm, and d = 2 μm. With the defined parameters and the established model, the simulation successfully calculated the reflectance of the SRM as shown in Fig. 1(c). The modes α_1, α_2, α_3, and α_4 are identical transverse mode with different longitudinal mode numbers and reflectance of approximately 0.9. The high reflectance modes of the microcavity facilitate efficient coupling to the FP cavity. In addition, the high reflectance means that the scattering loss at the sidewalls is low. The modes α_2 and α_3 at 1531.9 and 1548.8 nm are spaced 16.7 nm apart, corresponding to the longitudinal mode spacing of the microcavity.

Narrow linewidth lasers were fabricated using AlGaInAs/InP epitaxial wafer. The MQWs active layer is composed of three compressively strained wells and four lattice-matched barriers. Compared to HSRLs [7] and HSRRLs [8] prepared with 6-quantum wells epitaxial wafers, HSRRLs prepared with 3-quantum wells epitaxial wafers substantially reduce the confinement factor and facilitate the narrowing of the linewidth. The patterns of an HSRRL with the SRM side length a = 15 μm, the vertex extending distance δ = 0.82 μm, and FP cavity width d = 2 μm are defined by standard projection i-line lithography. The depth of patterns is about 4.5 μm by inductively coupled plasma (ICP) etching techniques. Fig. 1(d) shows the scanning electron microscopic (SEM) images of an HSRRL after ICP etching. To ensure low scattering losses, steep and smooth sidewalls are obtained by optimized lithography and ICP etching techniques. The ohmic contact layer between the SRM and the FP cavity is etched to guarantee mutual electrical isolation. The device is mounted on an AlN submount for measurement with the temperature controlled by a thermoelectric cooler (TEC). Continuous-wave (CW) injection currents are applied to the SRM and the FP cavity separately. The output light power is collected by a tapered single-mode fiber (SMF).

III. RESULTS AND DISCUSSIONS

The light-current-voltage (L-I-V) characteristics of the HSRRL are plotted in Fig. 2(a). The L-I-V curve exhibits a threshold current of 13 mA, a maximum SMF coupled output power of 10 mW at an FP injection current of 121 mA, and a slope efficiency of about 0.12 mW/mA for I_{SRM} = 2 mA at room temperature. A series resistance of 6.9 Ω is estimated from the V-I curve. The emission optical spectra are characterized by an optical spectrum analyzer to investigate the mode behaviors of the laser. Fig. 2(b) shows the lasing spectra at I_{SRM} = 3 mA and I_{FP} = 101 mA with a resolution of 0.01 nm. Single mode lasing at 1546.2nm with a sidemode suppression ratio (SMSR) of approximately 38 dB is obtained. Due to the wide reflectance spectrum of the SRM, the lasing spectrum exhibits high side modes and the envelope of the lasing spectrum corresponds to the reflectance spectrum. The two peaks marked by triangles at 1530.6 and 1546.2 nm are the same order transverse modes as the adjacent longitudinal modes of the SRM, showing a longitudinal mode spacing of 15.4 nm, which is in general agreement with the simulation.

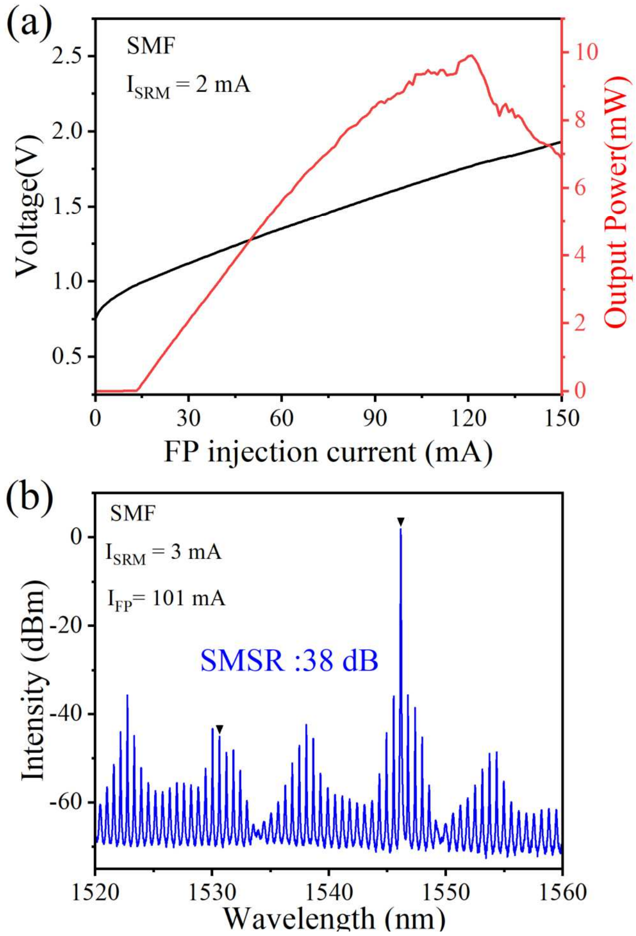

Fig. 2. (a) Applied voltage and SMF coupled power versus I_{FP} at fixed I_{SRM} of 22 mA. (b) Lasing spectra for the HSRRL at I_{SRM} = 3 mA and I_{FP} = 101 mA with a resolution of 0.01 nm.

We characterized the laser frequency noise based on the self-homodyne optical coherent receiver method [10]. The frequency noise measurement at I_{SRM} = 10 mA and I_{FP} = 123 mA is plotted in Fig. 3(a). At the lower frequency range, the noise spectrum is dominated by random walk frequency modulation (FM) noise and flicker FM noise [11]. In the flat section, the frequency noise is dominated by the white FM noise, from which the Lorentzian linewidth of the laser can be determined [12]. The ~1.6×10^5 Hz^2/Hz frequency noise near 5×10^8 Hz was obtained, indicating ~500 kHz linewidth of the Lorentz spectrum. Fig. 3(b) shows the linewidths of the HSRRL as a function of bias currents I_{FP} and I_{SRM}. When keeping I_{SRM} at 3 mA and raising I_{FP} from 40 to 123 mA, the linewidth becomes smaller due to the increase in photon number density. Similarly, when keeping I_{FP} at 123mA and raising I_{SRM}, the linewidth decreases. However, when the power is oversaturated, the linewidth becomes larger again. The minimum linewidth of 500 kHz is obtained at I_{SRM} = 10 mA and I_{FP} = 123 mA.

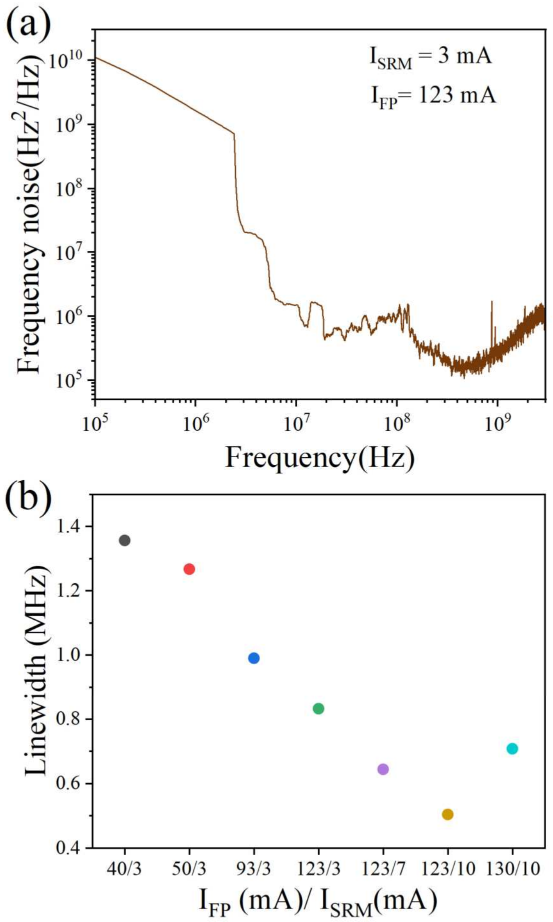

Fig. 3. (a) Frequency noise spectrum of the fabricated HSRRL at I_{SRM} = 10 mA and I_{FP} = 123 mA. (b) Measured linewidths versus bias currents.

IV. Conclusion

To conclude, we have demonstrated a narrow linewidth HSRRL based on a 3-quantum wells epitaxial wafer to reduce the longitudinal confinement factor. An SMF coupling output power of 10 mW and a linewidth of 500 kHz were achieved. Next, we will continue to narrow linewidth and increase output power to meet the demands of coherent optical communications.

References

[1] D. S. Ly-Gagnon, S. Tsukamoto, K. Katoh, and K. Kikuchi, "Coherent Detection of Optical Quadrature Phase-Shift Keying Signals With Carrier Phase Estimation," J. Lightwave Technol., vol. 24, no. 1, pp. 12-21, January 2006.

[2] K. H. Zou et al., "Higher-order QAM data transmission using a high-coherence hybrid Si/III-V semiconductor laser," Opt. Lett., vol. 45, no. 6, pp. 1499-1502, March 2020.

[3] E. Dale et al., "Ultra-Narrow Line Tunable Semiconductor Lasers for Coherent LIDAR Applications," in Imaging and Applied Optics 2014, Seattle, Washington, Optica Publishing Group, in OSA Technical Digest, 2014, Art. no. JTu2C.3.

[4] Z. L. Newman et al., "Architecture for the photonic integration of an optical atomic clock," Optica, vol. 6, no. 5, pp. 680-685, May 2019.

[5] D. Chang, O. Omomukuyo, X. Lin, S. Hang, O. A. Dobre, and R. Venkatesan, "Robust Faster-Than-Nyquist PDM-mQAM Systems With Tomlinson-Harashima Precoding," IEEE Photonics Technol. Lett., vol. 28, no. 19, pp. 2106-2109, October 2016.

[6] M. Seimetz and Osa, "Laser linewidth limitations for optical systems with high-order modulation employing feed forward digital carrier phase estimation," in Conference on Optical Fiber Communications/National Fiber Optic Engineers Conference, San Diego, CA, Optical Soc America, 2008, pp. 2470-2472.

[7] X. W. Ma, Y. Z. Huang, Y. D. Yang, J. L. Xiao, H. Z. Weng, and Z. X. Xiao, "Mode coupling in hybrid square-rectangular lasers for single mode operation," Appl. Phys. Lett., vol. 109, no. 7, Art. no. 071102, August 2016.

[8] Y. Z. Hao et al., "Widely tunable single-mode lasers based on a hybrid square/rhombus-rectangular microcavity," Photonics Res., vol. 7, no. 5, pp. 543-548, May 2019.

[9] V. Dhavamani, S. Chakraborty, S. Ramya, and S. Nandi, "Design and Simulation of Waveguide Bragg Grating based Temperature Sensor in COMSOL," Journal of Physics: Conference Series, vol. 2161, no. 1, Art. no. 012047, January 2022.

[10] K. Kikuchi and K. Igarashi, "Characterization of semiconductor-laser phase noise with digital coherent receivers," in 2011 Optical Fiber Communication Conference and Exposition and the National Fiber Optic Engineers Conference, March 2011, pp. 1-3.

[11] M. A. Tran, D. Huang, and J. E. Bowers, "Tutorial on narrow linewidth tunable semiconductor lasers using Si/III-V heterogeneous integration," APL Photonics, vol. 4, no. 11, Art. no. 111101, Nov 2019.

[12] L. A. Coldren, S. W. Corzine, and M. L. Mashanovitch, Diode lasers and photonic integrated circuits. 2nd ed. John Wiley & Sons, 2012, pp. 303-308.